Alternatively Spliced α_{1G} ($Ca_V3.1$) Intracellular Loops Promote Specific T-Type Ca^{2+} Channel Gating Properties

Jean Chemin, Arnaud Monteil, Emmanuel Bourinet, Joël Nargeot, and Philippe Lory
Institut de Génétique Humaine-CNRS UPR 1142–141, F-34396 Montpellier, France

ABSTRACT At least three genes encode T-type calcium channel α_1 subunits, and identification of cDNA transcripts provided evidence that molecular diversity of these channels can be further enhanced by alternative splicing mechanisms, especially for the α_{1G} subunit ($Ca_V3.1$). Using whole-cell patch-clamp procedures, we have investigated the electrophysiological properties of five isoforms of the human α_{1G} subunit that display a distinct III-IV linker, namely, $\alpha_{1G\text{-}a}$, $\alpha_{1G\text{-}b}$, and $\alpha_{1G\text{-}bc}$, as well as a distinct II-III linker, namely, $\alpha_{1G\text{-}ae}$, $\alpha_{1G\text{-}be}$, as expressed in HEK-293 cells. We report that insertion e within the II-III linker specifically modulates inactivation, steady-state kinetics, and modestly recovery from inactivation, whereas alternative splicing within the III-IV linker affects preferentially kinetics and voltage dependence of activation, as well as deactivation and inactivation. By using voltage-clamp protocols mimicking neuronal activities, such as cerebellar train of action potentials and thalamic low-threshold spike, we describe that inactivation properties of $\alpha_{1G\text{-}a}$ and $\alpha_{1G\text{-}ae}$ isoforms can support channel behaviors reminiscent to those described in native neurons. Altogether, these data demonstrate that expression of distinct variants for the T-type α_{1G} subunit can account for specific low-voltage-activated currents observed in neuronal tissues.

INTRODUCTION

Voltage-dependent Ca^{2+} channels (VDCCs) are a major pathway for rapid influx of Ca^{2+} into cells, involved in both electrical and metabolic signaling. Electrophysiological studies have identified two primary channel types, high-voltage-activated (HVA) and low-voltage-activated (LVA) channels (Carbone and Lux, 1984; Bean, 1989). For LVA Ca^{2+} channels, generally designated T-type channels, significant functional differences have been observed in native tissues particularly in inactivation kinetics and in the voltage dependence of steady-state inactivation (for review, see Huguenard 1996). Recently, three genes encoding T-type VDCC α_1 subunits have been identified (Perez-Reyes et al., 1998; Cribbs et al., 1998; Lee et al., 1999; Williams et al., 1999; Klugbauer at al., 1999; Monteil et al., 2000a,b) providing a basis for molecular diversity of T-type VDCCs. Functional expression of these channel subunits (α_{1G}, α_{1H}, and α_{1I}) has clearly demonstrated that the biophysical properties of T-type channels generated by α_{1G}, α_{1H}, and α_{1I} subunits are markedly different (Kozlov et al., 1999; Klockner et al., 1999; Monteil et al., 2000b) and could support specific Ca^{2+} entry profiles reminiscent of those recorded on native cells (Chen and Hess 1990; Zhuravleva et al., 1999). In addition, the existence of several isoforms for each of the α_{1G}, α_{1H}, and α_{1I} subunits was also established, indicating that there is an additional step that further increases the molecular diversity of T-type VDCCs (Mittman et al., 1999a,b; Monteil et al. 2000a,b). Regarding HVA Ca^{2+} channels, several studies have demonstrated that isoforms encoding L-type channels (Soldatov et al., 1997) and N-type channels (Lin et al., 1999) can exhibit specific activities. Two functionally distinct splice variants of the α_{1A} subunit encode the P- and Q-type Ca^{2+} channels (Bourinet et al., 1999). For the human α_{1G} subunit ($Ca_V3.1$), at least seven regions of the molecule with sequence variation were found (Mittman et al., 1999b; Monteil et al., 2000a; Cribbs et al., 2000), including the intracellular loops between domains II and III (skipping of exon 16, i.e., region *e*) and domains III and IV (alternative splicing of exon 25, i.e., *a*/*b*, and skipping of exon 26, i.e., *c*). In addition, we have recently shown that there is tissue-specific expression of these α_{1G} isoforms with the *a* isoforms ($\alpha_{1G\text{-}a}$ and $\alpha_{1G\text{-}ae}$) being preferentially expressed in neuronal tissues (Monteil et al., 2000a; Dubin et al., 2000). Here we have expressed in HEK-293 cells five α_{1G} isoforms including exon 16 within the II-III linker, namely, $\alpha_{1G\text{-}ae}$ and $\alpha_{1G\text{-}be}$, as well as a distinct III-IV linker, namely, $\alpha_{1G\text{-}a}$, $\alpha_{1G\text{-}b}$, and $\alpha_{1G\text{-}bc}$, and compared their functional properties using a whole-cell configuration of the patch-clamp technique. We have found several differences in the kinetics and steady-state properties among these α_{1G} isoforms that demonstrate that intracellular loops of the T-type α_{1G} subunit play an important role in generating functional heterogeneity of T-type Ca^{2+} channels. A preliminary account of this work has been presented at the Biophysical Meeting in New Orleans (Monteil et al., 2000c).

Received for publication 19 July 2000 and in final form 18 December 2000.
Address reprint requests to Dr. Philippe Lory, IGH-CNRS UPR 1142–141, rue de la Cardonille, F-34396 Montpellier cedex 05, France. Tel.: 33-0-499-61-99-36; Fax: 33-0-499-61-99-01; E-mail: philippe.lory@igh.cnrs.fr.

0006-3495/01/03/1238/13 $2.00

MATERIALS AND METHODS

Cloning of human α_{1G} subunit isoforms

Complementary DNA fragments were cloned by reverse transcriptase polymerase chain reaction (RT-PCR) from a variety of human mRNA samples as described in Monteil et al. (2000a). The novel isoforms encoding for the α_{1G} subunit, designated $\alpha_{1G\text{-}bc}$, $\alpha_{1G\text{-}ae}$, and $\alpha_{1G\text{-}be}$, were con-

structed from the original isoforms $\alpha_{1G\text{-}a}$ (Genbank accession number AF126966) and $\alpha_{1G\text{-}b}$ (AF126965). Briefly, the region encoding variation *e* was inserted in cDNAs encoding $\alpha_{1G\text{-}a}$ and $\alpha_{1G\text{-}b}$ isoforms using the unique restriction sites SpeI (nt 1993; AF126965) and *Xho*I (nt 3851) to produce the $\alpha_{1G\text{-}ae}$ and $\alpha_{1G\text{-}be}$ isoforms (AF227744 and AF227751, respectively). Similarly, the $\alpha_{1G\text{-}bc}$ isoform (AF227747) was constructed using the *Xho*I and *Bst*EII (nt 4927) restriction sites. These cDNAs were then subcloned in the mammalian expression vector pBK-CMV (Stratagene, La Jolla, CA) and sequenced using automatic sequencing (Applied Biosystems).

Cell culture and transient transfection

Human embryonic kidney cells HEK-293 were grown in Dulbecco's modified Eagle's medium (Eurobio) supplemented with 10% fetal bovine serum and 1% penicillin/streptomycin (v/v). One day before transfection, cells were plated at 70–90% confluence on a 35-mm petri dish. A standard Ca^{2+} phosphate procedure was performed with 0.3 μg of a plasmid encoding the reporter gene GFP and 2.7 μg of different pBK-CMV constructs that encode for the α_{1G} isoforms: α_{1Ga}, α_{1Gb}, α_{1Gbc}, α_{1Gae}, and α_{1Gbe}. Cells were then plated at low confluence, and whole-cell recordings were made 1–4 days after transfection.

Electrophysiology

Macroscopic currents were recorded by the whole-cell patch-clamp technique at room temperature using an Axopatch 200B amplifier. Records were filtered at 5 kHz and capacitive currents were subtracted using a P/-5 procedure when needed, i.e., for tail current recordings and action potential clamps. Extracellular solution contained (in mM): 2 $CaCl_2$, 160 tetraethylammonium chloride, 10 HEPES (pH to 7.4 with tetraethylammonium hydroxide). Pipettes made of borosilicate glass with a typical resistance of 1–2 MΩW were filled with an internal solution containing (in mM): 110 CsCl, 10 EGTA, 10 HEPES, 3 Mg-ATP, 0.6 GTP (pH to 7.2 with CsOH). For action potential clamp we have used 1) a generic action potential (J. Pancrasio, Axon Instruments web site), 2) a train of spikes typical of that recorded in Purkinje neurons of the cerebellum generously provided by Dr. B. P. Bean (Havard Medical School, Boston, MA), and 3) a low-threshold spike (LTS) typical of those measured on thalamic relay neurons. The LTS was generated using the NEURON model (Hines and Carnevale, 1997) adapted by Destexhe et al. (1998) for thalamo-cortical relay cells. The parameters used in our experiments (three-compartment model configuration of burst behavior) were downloaded from the model database at Yale University (http://senselab.med.yale.edu/senselab/neurondb/). With this model, a LTS was produced by a 45-pA current stimulation during 200 ms, then converted into a pCLAMP stimulation file, and further applied to the HEK-293 cells. Data were acquired on a PC and were analyzed (see below) using pCLAMP6 (Axon Instruments, Foster City, CA), Excel (Microsoft), and GraphPad Prism (GraphPad) softwares.

Electrophysiological analysis

Current-voltage curves (*I-V* curves) were fitted using a combined Boltzmann and linear ohmic relationships, where $I = G_{max} \times (V_m - V_{rev})/(1 + e^{(Vm-V1/2)/slope})$. To minimize the consequence of current rectification near reversal potential on the determination of conductance, the current values greater than +10 mV were not considered for the fit. The normalized conductance-voltage curves were fitted with a Boltzmann equation: $G/G_{max} = 1/(1 + e^{(V1/2-Vm)/slope})$. Similarly, steady-state inactivation curves were fitted using $I/I_{max} = 1 - 1/(1 + e^{(V1/2-Vm)/slope})$. Kinetics of the recovery from inactivation were calculated with a double-exponential expression: $\%I = A_1 (1 - e^{-Vm/\tau 1}) + A_2 (1 - e^{-Vm/\tau 2})$ where A_1 and A_2 are the relative amplitudes of each exponential and τ_1 and τ_2 their respective time constants. To better evaluate the role of each channel isotype on the recovery process, we defined the global recovery (τ_g) as $A_1\tau_1 + A_2\tau_2$. Time constants (τ) of inactivation and deactivation were extracted from monoexponential fit while the rate of activation was estimated by the time for a rise of the current from 10% to 90% (see also Randall and Tsien, 1997). The rise 10–90 measurement of the activation rate limits contamination by the inactivation process. Time constant of deactivation was plotted versus membrane potential (V_m) using the following equation: $\tau_{deac} = e^{((Vm-Vmin)/e\text{-}fold)}$, where V_{min} corresponds to the more negative test potential (−120 mV) used in our experiments. Similar curves for activation (rise 10–90) and inactivation (time constant) were obtained using (rise 10–90) = (rise 10–90)$_{max} \times e^{(-Vm/e\text{-}fold)}$ + (rise 10–90)$_{min}$ and $\tau = \tau_{max} \times e^{(-Vm/e\text{-}fold)} + \tau_{min}$, respectively. One-way ANOVA combined with a Student-Newman-Keuls post-test were used to compare the different values and were considered significant at $p < 0.05$. Results are presented as the mean ± SEM, and *n* is the number of cells used.

RESULTS

To investigate the role of the two intracellular linkers between domains II and III as well as between domains III and IV, several natural isoforms of the human α_{1G} subunit encoding distinct II-III and III-IV loops were constructed and subcloned into the mammalian expression vector pBK-CMV. The molecular cloning of the corresponding cDNA fragments has been described previously in Monteil et al. (2000a), and the various isoforms were named $\alpha_{1G\text{-}a}$, $\alpha_{1G\text{-}b}$, $\alpha_{1G\text{-}bc}$, $\alpha_{1G\text{-}ae}$, and $\alpha_{1G\text{-}be}$ (Fig. 1). When expressed in HEK-293 cells, all these α_{1G} subunit isoforms produced robust typical T-type Ca^{2+} currents. We first analyzed the voltage dependence of each of these Ca^{2+} currents by plotting the normalized current density as a function of the membrane depolarization (*I-V* curve). Because we focused our attention only on the activation phase of the *I-V* curves, we have fitted the *I-V* curves with a combined Boltzmann and linear ohmic relationships (see Materials and Methods), although a Goldman-Hodgkin-Katz relationship would have been more adapted to account for the rectification of the current amplitude near its reversal potential. For this analysis, current traces were recorded using a large range of depolarizing test pulses (TPs; from −90 to +50 mV) of short duration (100 ms) from the holding potential (HP) at −110 mV. Fig. 2 *A* shows typical recordings of the currents generated by the $\alpha_{1G\text{-}a}$ subunit. Scaled *I-V* curves indicated that the $\alpha_{1G\text{-}a}$ and $\alpha_{1G\text{-}ae}$ currents activated more negatively than those generated by the three other isoforms (Fig. 2 *B*). These currents activated around −70 mV and peaked at −36 ± 1 mV (see Table 1), whereas $\alpha_{1G\text{-}b}$, $\alpha_{1G\text{-}be}$, and $\alpha_{1G\text{-}bc}$ currents activated around −60 mV and peaked around −31 ± 1 mV (see Table 1). Steady-state activation properties were deduced from the plot of the normalized conductance-voltage (*G-V*) curves (Fig. 2 *C*). The deduced half-maximal activation values ($V_{0.5}$) and the slope factors (*k*, in mV) for the five experimental conditions are reported in Table 1. Altogether these data indicated that the $\alpha_{1G\text{-}a}$ and $\alpha_{1G\text{-}ae}$ currents activated significantly more negatively (~5 mV; $p < 0.001$) than those generated by the $\alpha_{1G\text{-}b}$, $\alpha_{1G\text{-}be}$, and $\alpha_{1G\text{-}bc}$ subunits, suggesting an important role for activation

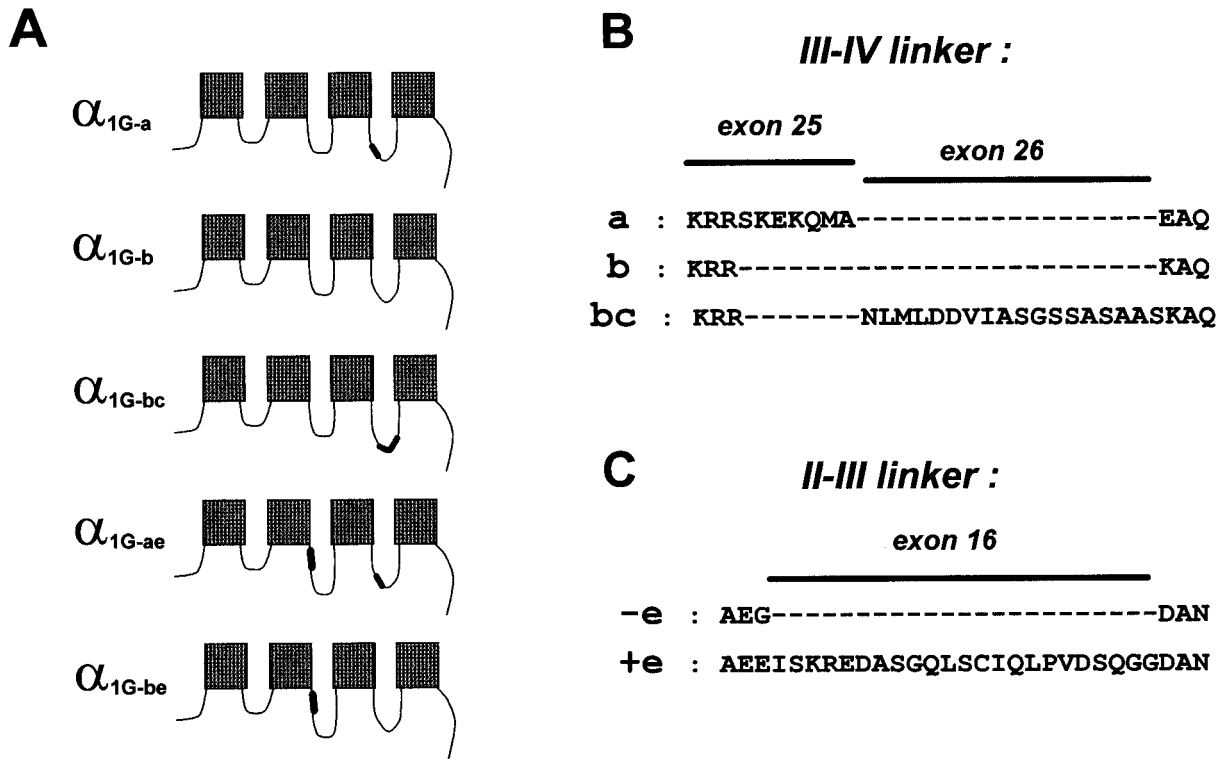

FIGURE 1 A comprehensive scheme of the isoforms of α_{1G} subunit. (*A*) The isoforms of the α_{1G} subunit are named according to their differences in amino acid content in the intracellular III-IV (isoforms α_{1G-a}, α_{1G-b}, and α_{1G-bc}) and II-III loops (isoforms α_{1G-ae} and α_{1G-be}). Note that the α_{1G-b} isoform corresponds to the shortest polypeptide encoding the α_{1G} subunit. (*B*) Amino acid structure of the III-IV linker. Alternative splicing of exon 25 generates two isoforms named α_{1G-a} and α_{1G-b}. For a detailed analysis of the splicing mechanism of exon 25 see Monteil et al., 2000a). The use of exon 26 is involved in the generation of insertion *c* encoding 16 amino acids, which is retrieved only in association with the *b* variation (α_{1G-bc}) in humans. (*C*) Amino acid structure of the II-III linker. The alternative use of exon 16 is responsible for insertion *e*, a 23-amino-acid stretch, which was found associated with the *a* as well as the *b* variations.

of the seven-amino-acid stretch found in the α_{1G-a} and α_{1G-ae} isoforms.

Fig. 3 *A* provides a comparison of the current traces recorded at −40 mV (*upper panel*) and −10 mV (*lower panel*) generated by the five α_{1G} isoforms. It illustrates that both activation and inactivation kinetics were markedly different at negative potentials (−40 mV). At more positive membrane potentials (−10 mV) activation and inactivation kinetics tended to normalize for α_{1G-a}, α_{1G-b}, and α_{1G-bc} currents, whereas α_{1G-ae} and α_{1G-be} currents exhibited faster inactivation rates. A plot of activation kinetics (rise 10–90, Fig. 3 *B*) and inactivation kinetics (time constant, Fig. 3 *C*) as a function of the TP potentials showed that activation and inactivation kinetics were strongly voltage dependent for all channel types in the negative range of membrane potential (−55 to −10 mV). Although accurate activation kinetics measurements of T-type currents are difficult to obtain due to possible contamination by their rapid inactivation rate, it should be noted, however, that for negative membrane potentials (i.e., at −40 mV where inactivation rates were moderately different for all the currents), α_{1G-a} and α_{1G-ae} currents exhibited significantly faster activation rates than α_{1G-b} and α_{1G-be} currents, respectively ($p < 0.001$); also Table 1). By contrast, above −30 mV where no differences in activation kinetics were observable among the currents generated by the five isoforms, α_{1G-ae} and α_{1G-be} currents exhibited significantly faster inactivation rates (~11ms) as compared with α_{1G-a} and α_{1G-b} currents (~15ms), respectively (see Table 1).

The steady-state voltage-dependent inactivation was determined by varying the voltage level of a 5-s conditioning pulse applied before a 100-ms TP at −30 mV (Fig. 4 *A*). Normalized amplitudes of the currents generated by the five α_{1G} isoforms were plotted as a function of the membrane potential of the conditioning pulse. The voltage dependence of the steady-state inactivation for each experimental condition can be best described by a single Boltzmann equation (Fig. 4 *A*). The deduced half-maximal inactivation values $V_{0.5}$ and the slope factor k for the five experimental conditions are presented in Table 1. The $V_{0.5}$ values obtained for α_{1G-ae} and α_{1G-be} currents were significantly different from α_{1G-a} and α_{1G-b} currents according to an unpaired Student *t*-test ($p < 0.01$). Similarly, the $V_{0.5}$ values obtained for the α_{1G-a}, α_{1G-b}, and α_{1G-bc} currents were significantly different

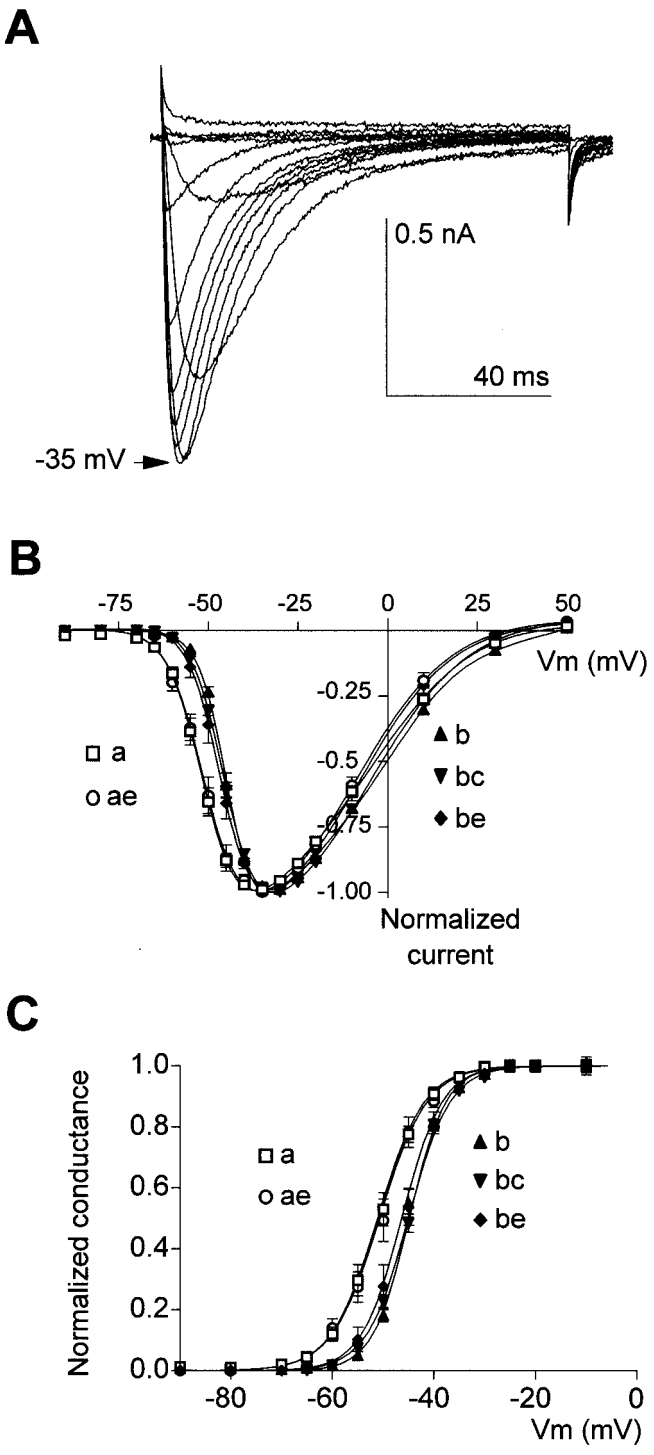

FIGURE 2 Steady-state activation properties. (*A*) Typical Ca^{2+} currents, generated here by the $\alpha_{1G\text{-a}}$ isoform, were obtained by increasing the depolarization steps from −90 to +50 mV of a 100-ms test pulse (TP) from a holding potential (HP) of −110 mV. (*B*) Average current-voltage (*I-V*) relationship for the various α_{1G} isoforms. For each *I-V* relationship, the line corresponds to a smooth curve, which accounts for the Ca^{2+} current measurements. (*C*) For the determination of the activation parameters, each *I-V* relationship was fitted according to the procedure described in Materials and Methods. Normalized conductance curves for the various α_{1G} isoforms were then constructed. Note the negative 5-mV shift for the *a* isoforms compared with the *b* isoforms.

($p < 0.01$). Altogether, these results indicated that the II-III and III-IV linkers are both involved in the inactivation process of the α_{1G} current.

The time dependence of the recovery from short-term inactivation was estimated using a two-pulse protocol separated with an inter-pulse interval of variable duration (Fig. 4 *B*). These recovery plots, which present the normalized current amplitude as a function of inter-pulse duration, were best fitted, for each isoform, with the sum of two exponentials that resolved two distinct time constants. Therefore, to better evaluate the recovery properties for each channel isotype, we have defined the global recovery τ_g as $A_1\tau_1 + A_2\tau_2$ (Fig. 4 *C*). Recovery of $\alpha_{1G\text{-b}}$ currents recorded at HP −110 mV was significantly faster than that of $\alpha_{1G\text{-a}}$ and $\alpha_{1G\text{-bc}}$ currents (Fig. 4 *C*). In addition, recovery of $\alpha_{1G\text{-a}}$ and $\alpha_{1G\text{-b}}$ was significantly faster than that of $\alpha_{1G\text{-ae}}$ and $\alpha_{1G\text{-be}}$ currents, indicating that the intracellular loops between domain II-III and III-IV both modulate the recovery-from-inactivation process of the α_{1G} current. When switching from HP −110 mV to HP −70 mV, recovery was two- to fourfold slower for each current isotype, and global recovery was no longer significantly different between each current isotype (Fig. 4 *C*), indicating that recovery from short-term inactivation normalized in the range of physiological resting membrane potential.

Deactivation properties of currents generated by these five α_{1G} isoforms were also analyzed. Currents were elicited using an 8-ms pulse to −30 mV and their deactivation was measured during membrane repolarization to potentials ranging from −120 to −50 mV (Fig. 5 *A*, *inset*). At each voltage, deactivation kinetics was best described with a single exponential function for each channel isotype. At −120 mV, deactivation kinetics was as fast as 2 ms for each current type. Time constant values were plotted as a function of the repolarizing potential that clearly indicated that the deactivation kinetics was voltage dependent for any of the channel types (Fig. 5 *A*). Above −100 mV, deactivation kinetics was significantly faster for currents generated by $\alpha_{1G\text{-b}}$ and $\alpha_{1G\text{-be}}$, as compared with $\alpha_{1G\text{-a}}$, $\alpha_{1G\text{-ae}}$, and $\alpha_{1G\text{-bc}}$, indicating a role for the III-IV linker in the deactivation process. Whether distinct deactivation kinetics would influence channel behavior was further evaluated on currents evoked using action potential (AP) clamp protocol (Fig. 5 *B*). Superimposition of currents generated by the $\alpha_{1G\text{-b}}$, $\alpha_{1G\text{-ae}}$, and $\alpha_{1G\text{-bc}}$ isoforms using a fast (2-ms) AP clearly revealed that $\alpha_{1G\text{-bc}}$, which exhibited the slowest deactivation kinetics, contributed to a more sustained inward Ca^{2+} current (Fig. 5 *B*). Such an effect was quantified by calculating the average ratio of the amplitude of the current 10 ms after the triggering of the AP (I_{10ms}) to the maximum of the current amplitude for the AP (I_{max}) in each situation (I_{10ms}/I_{max} = AP ratio; Fig. 5 *C*). These calculations indicated that $\alpha_{1G\text{-b}}$ isoform induced an inward current (ratio 0.14 ± 0.01, $n = 15$) significantly more transient than for $\alpha_{1G\text{-ae}}$ (ratio 0.25 ± 0.02, $n = 10$) and $\alpha_{1G\text{-bc}}$ (ratio

Table 1 Electrophysiological parameters describing the various α_{1G} isoforms

	α_{1Ga}		α_{1Gae}		α_{1Gb}		α_{1Gbe}		α_{1Gbe}		α_{1Ga}/ α_{1Gae}	α_{1Ga}/ α_{1Gb}	α_{1Gb}/ α_{1Gbc}
	Mean ± SEM	*n*	Mean ± SEM	*n*	Mean ± SEM	*n*	Mean ± SEM	*n*	Mean ± SEM	*n*			
Activation													
Pic (mV)	−36 ± 1	10	−36.2 ± 1.3	13	−31 ± 0.9	10	−32 ± 1	10	−30.5 ± 0.9	10	—	**	—
$V_{1/2}$ (mV)	−51.2 ± 0.9	10	−50.7 ± 1.1	13	−44.7 ± 0.6	10	−46.3 ± 1	10	−45 ± 0.4	10	—	***	—
Slope (mV)	4.6 ± 0.1	10	4.7 ± 0.12	13	3.6 ± 0.22	10	3.9 ± 0.11	10	4 ± 0.13	10	—	***	—
Inactivation													
$V_{1/2}$ (mV)	−74.7 ± 0.4	10	−80.6 ± 0.4	10	−65 ± 0.4	10	−70.5 ± 0.8	10	−71.1 ± 0.5	10	***	***	***
Slope (mV)	5.4 ± 0.3	10	5.3 ± 0.1	10	4.4 ± 0.1	10	4.9 ± 0.2	10	4.2 ± 0.2	10	—	**	—
Kinetics													
Activation													
Rise −40 mV (ms)	4 ± 0.2	10	3.9 ± 0.3	13	7.3 ± 0.3	10	5.7 ± 0.2	10	5.1 ± 0.4	10	—	***	***
Rise −10 mV (ms)	1.42 ± 0.1	10	1.3 ± 0.09	13	1.67 ± 0.08	10	1.45 ± 0.15	10	1.5 ± 0.1	10	—	—	—
e-fold (mV)	12.8 ± 1	10	10.9 ± 1.1	13	13.4 ± 1.5	10	12 ± 2.8	10	11.9 ± 0.9	10	—	—	—
Inactivation													
Tau −40 mV (ms)	17 ± 1.3	10	14.3 ± 0.5	13	21.8 ± 0.9	10	18.2 ± 1.5	10	20.8 ± 1.2	10	—	*	—
Tau −10 mV (ms)	15.1 ± 0.9	10	11.1 ± 0.3	13	15.4 ± 0.8	10	11.5 ± 0.6	10	15.6 ± 0.3	10	***	—	—
e-fold (mV)	8.9 ± 1.8	10	8.5 ± 0.9	13	4.8 ± 0.6	10	7.4 ± 1.2	10	6.9 ± 0.8	10	—	—	—
Deactivation													
Tau −70 mV (ms)	7.3 ± 0.9	10	7 ± 0.8	10	4.2 ± 0.2	10	4.4 ± 0.3	10	8 ± 1.2	10	—	*	*
e-fold (mV)	33.4 ± 1.5	10	35.2 ± 0.7	10	35.5 ± 1.5	10	34.3 ± 0.4	10	34.7 ± 0.7	10	—	—	—

Values are expressed as mean ± SEM and *n* is the numbers of cells used.
Statistical comparison of $\alpha_{1G\text{-}a}$ versus $\alpha_{1G\text{-}ae}$, $\alpha_{1G\text{-}a}$ versus $\alpha_{1G\text{-}b}$, and α_{1Gb} versus $\alpha_{1G\text{-}bc}$ were done using a one-way ANOVA followed by a Student–Newman–Keuls post test with $*P < 0.05$, $**P < 0.01$, and $***P < 0.001$.

0.29 ± 0.02, $n = 10$). We also calculated for each channel isotype a ratio $I_{max\text{-}AP}/I_{max\text{-}TP}$ corresponding to the maximum of the current amplitude induced by the AP ($I_{max\text{-}AP}$) over the maximum peak current amplitude recorded for −30 mV TP at HP −110 mV ($I_{max\text{-}TP}$). This ratio describes the ability of a given channel isoform to open, i.e., its availability, during the AP. The $I_{max\text{-}AP}/I_{max\text{-}TP}$ ratio values indicated that $\alpha_{1G\text{-}b}$ and $\alpha_{1G\text{-}be}$ channel availability during an AP was significantly larger (2.45 ± 0.11, $n = 15$, and 2.01 ± 0.18, $n = 10$) than for $\alpha_{1G\text{-}a}$ and $\alpha_{1G\text{-}ae}$ channels (1.49 ± 0.12, $n = 10$, and 1.2 ± 0.15, $n = 10$, respectively). In addition, availability of $\alpha_{1G\text{-}bc}$ channels (1.77 ± 0.2, $n = 10$) was significantly smaller than for $\alpha_{1G\text{-}b}$ channels (data not shown). These results clearly indicated that the amplitude of the AP-induced current is primarily dependent on the steady-state inactivation properties, whereas the time course of the Ca^{2+} entry is more related to the deactivation kinetics. Altogether, these data confirmed that α_{1G} channels allow a massive Ca^{2+} entry during neuronal APs (Monteil et al., 2000a; Lambert et al., 1998) and suggested that the α_{1G} isoforms exhibit specific behavior that can be better analyzed using dynamic AP voltage-clamp protocols.

As a first step toward evaluating whether the biophysical differences described for the various α_{1G} isoforms would result in distinct contributions to the voltage-dependent influx of Ca^{2+}, we have examined the activity of the neuronal isoforms $\alpha_{1G\text{-}a}$ and $\alpha_{1G\text{-}ae}$, by comparison with the $\alpha_{1G\text{-}b}$ isoform, using voltage-clamped neuronal activities. First we used a mimicked LTS from thalamic neurons where the role of T-type channels in promoting burst activity is well described (Destexhe et al., 1998). The HEK-293 cells expressing Ca^{2+} currents of comparable amplitude at HP −110 mV (Fig. 6 *A*) were maintained at HP −74 mV before applying a LTS waveform in voltage clamp conditions (Fig. 6 *B*), typical of those recorded in thalamocortical relay cells (TC neurons). The resulting inward Ca^{2+} currents showed a bell-shaped time course that was of larger amplitude for *b* isoforms than for *a* isoforms (Fig. 6 *B*). The normalized LTS Ca^{2+} signals (LTS-induced Ca^{2+} current/ $I_{max\text{-}TP}$) was significantly larger for *b* isoforms than for *a* and *ae* isoforms (Fig. 6 *C*). These results strongly indicated that availability of each channel isotype during the development of LTS is primarily related to its steady-state inactivation properties.

We next probed the activity of these α_{1G} channel isotypes during a typical spike train voltage-clamp protocol. HEK-293 cells were maintained at HP −70 mV before applying a spike train as command voltage-clamp waveform (Fig. 7 *A*) recorded originally from a spontaneously firing (~50 Hz) isolated Purkinje neuron (Raman and Bean, 1999). Using this experimental protocol, inward Ca^{2+} currents peaked during the inter-spike intervals, at the repolarization phase, in good agreement with that described for isolated APs (Fig. 5). As illustrated in Fig. 7 *A*, the currents induced by the $\alpha_{1G\text{-}b}$, $\alpha_{1G\text{-}a}$, and $\alpha_{1G\text{-}ae}$ channels markedly differ in their initial amplitude, time course of the decay, and level of steady-state Ca^{2+} influx. The spike-induced currents were normalized to the maximum amplitude of the corresponding currents recorded at −110 mV ($I_{max\text{-}TP}$; Fig. 7 *A*), and plotted as a function of time to estimate the availability of

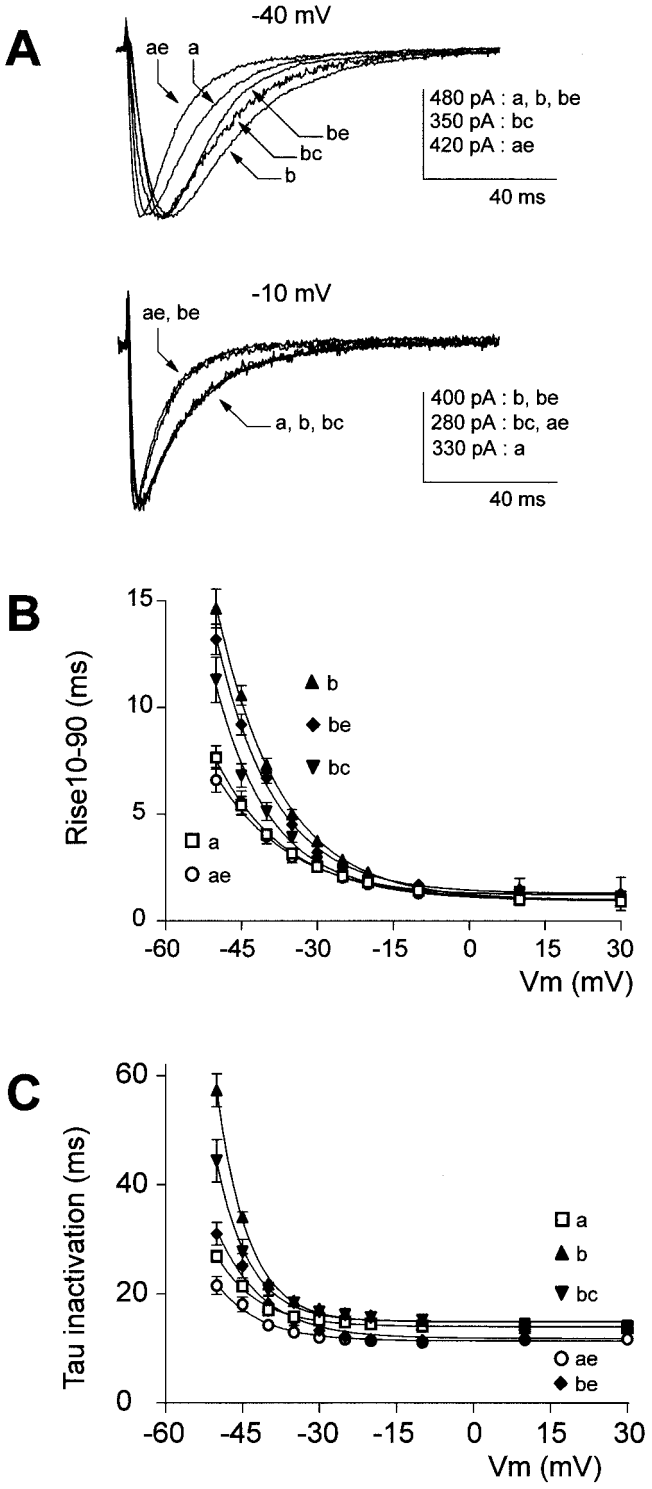

FIGURE 3 Activation and inactivation kinetics. (*A*) Typical currents evoked by a 100-ms TP to −40 mV (*upper panel*) and −10 mV (*lower panel*) from a HP of −110 mV for the various α_{1G} isoforms. (*B*) Activation kinetics (Rise 10–90) of the α_{1G} isoforms. Note that activation kinetics are similar for depolarization greater than −10 mV for the various α_{1G} isoforms. (*C*) Inactivation kinetics (time constant τ) of the Ca^{2+} currents generated by the various α_{1G} isoforms.

each channel isoform during such a typical firing activity of Purkinje neurons (Fig. 7 *B*). First, the initial current amplitude in response to the first spike was significantly higher for *b* isoforms than for *a* isoforms ($\alpha_{1G\text{-}b} > \alpha_{1G\text{-}a} \gg \alpha_{1G\text{-}ae}$), indicating that availability of each channel isotype at −70 mV was strongly related to its steady-state inactivation properties. Second, the time course of the decay in current amplitude was slower for *b* isoforms (76.9 ± 5.4 ms, $n = 11$) than for a isoforms (68.9 ± 3.7 ms, $n = 15$, for $\alpha_{1G\text{-}a}$ and 61.6 ± 5.4 ms, $n = 17$, for $\alpha_{1G\text{-}ae}$). Most likely, an inactivation process defined as cumulative inactivation could explain the time course of the current decay that is occurring during repetitive activities (Serrano et al., 1999). This phenomenon is related to the inactivation kinetics in association with the deactivation process (Kozlov et al., 1999).

Indeed, the *b* isoforms, which exhibited fast deactivation and slow inactivation kinetics compared with the *a* isoforms, were less inactivated during the inter-spike periods. Conversely, the *e* isoforms, which are characterized by rapid inactivation kinetics, were more inactivated during the inter-spike intervals. As a consequence, these experiments revealed that the presence of a steady-state inward Ca^{2+} current, which was observable after the 10th spike, was clearly dependent upon the α_{1G} isoform. Little steady Ca^{2+} current was associated with the *a* isoforms, especially with $\alpha_{1G\text{-}ae}$ channels, whereas a significant Ca^{2+} current remained in the case of the *b* isoforms (Fig. 7 *B*).

DISCUSSION

We describe here that the isoforms of the human α_{1G} subunit harboring distinct II-III and III-IV linkers display specific electrophysiological properties that determine markedly distinct behavior for each channel isotype. In this study, we have focused our attention on the biophysical properties of a subset of five isoforms of the human α_{1G} subunit that comprises the three sequence variations in the linkers between domains II and III and domains III and IV identified to date. We limited, however, our analysis to native isoforms of the α_{1G} subunit, and all the possible combinations of splice sequences were not examined. The five isoforms of the human α_{1G} subunit investigated here have been clearly identified by molecular cloning strategies (Monteil et al., 2000a). The specific roles of these regions of variation designated a/b (alternative splicing of exon 25), c (skipping of exon 26), and e (skipping of exon 16) in T-type Ca^{2+} channel activity has been determined by functional analysis. These results, together with our recent data describing tissue-specific expression of these isoforms (Monteil et al., 2000a), strongly suggest that alternative splicing of the α_{1G} subunit contributes to an important level of diversity of T-type Ca^{2+} channel signaling.

Examination of the genomic structure of the human CACNA1G gene as well as cDNA cloning experiments

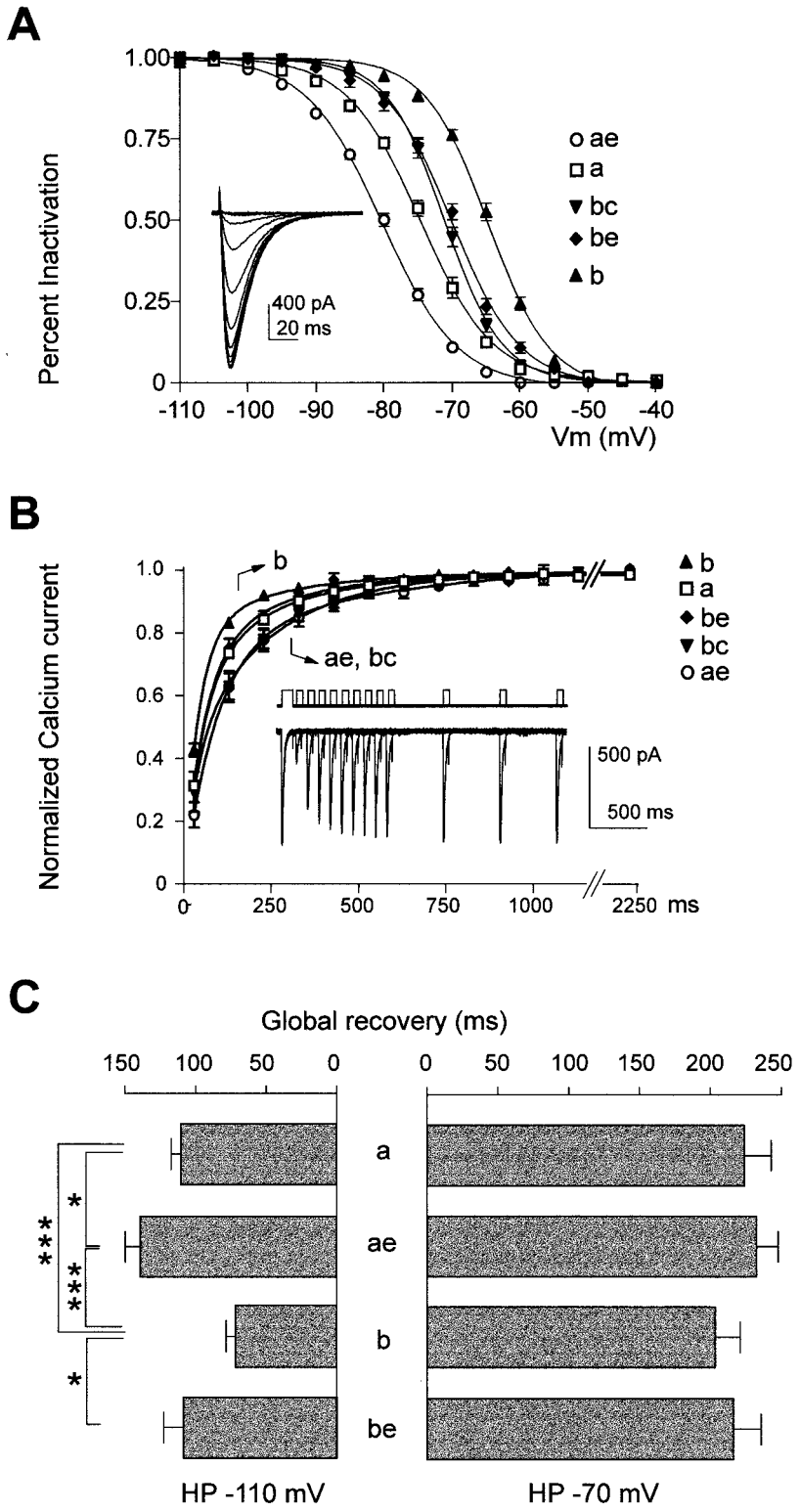

FIGURE 4 Steady-state inactivation and recovery from inactivation. (*A*) Steady-state inactivation curves for the various α_{1G} isoforms. The corresponding values are presented in Table 1. A typical example of $\alpha_{1G\text{-}a}$ currents evoked by a 100-ms depolarization TP to −30 mV elicited after a 5-s pre-depolarization pulse of increasing amplitude from −110 to −30 mV is presented in the inset. (*B*) Recovery from short-term inactivation of the α_{1G} isoforms. A two-pulse protocol (−30 mV TP) with various interpulse durations was used to measure the fast recovery kinetics as illustrated in the inset for the $\alpha_{1G\text{-}a}$ isoform. For all the isoforms the recovery time course is best fitted by the sum of two exponentials. At HP −110 mV, $\alpha_{1G\text{-}b}$ showed the fastest recovery whereas the isoforms *ae* and *bc* had the slowest recovery. (*C*) Recovery as a function of HP level. The global recovery, as defined in Materials and Methods (τ_G) was quantified at two HPs: −110 mV and −70 mV. The same protocol described above was performed on the transfected cells for HP −110 mV and HP −70 mV, and τ_G was determined. Note that for all the α_{1G} isoforms the recovery from short-term inactivation was similar in the range of physiological resting membrane potential (HP −70 mV).

have indicated that two versions only of the II-III linker of the α_{1G} subunit are likely to exist. They correspond to the alternative use of sequence e (23 amino acids) encoded by exon 16 (Mittman et al., 1999b; Monteil et al., 2000a). According to our long-range RT-PCR experiments (Monteil et al., 2000a), insertion e is found both in association with the a isoforms (~30%) and b isoforms (~20%). In human brain, the isoform $\alpha_{1G\text{-}ae}$ is found abundantly (~30%) and

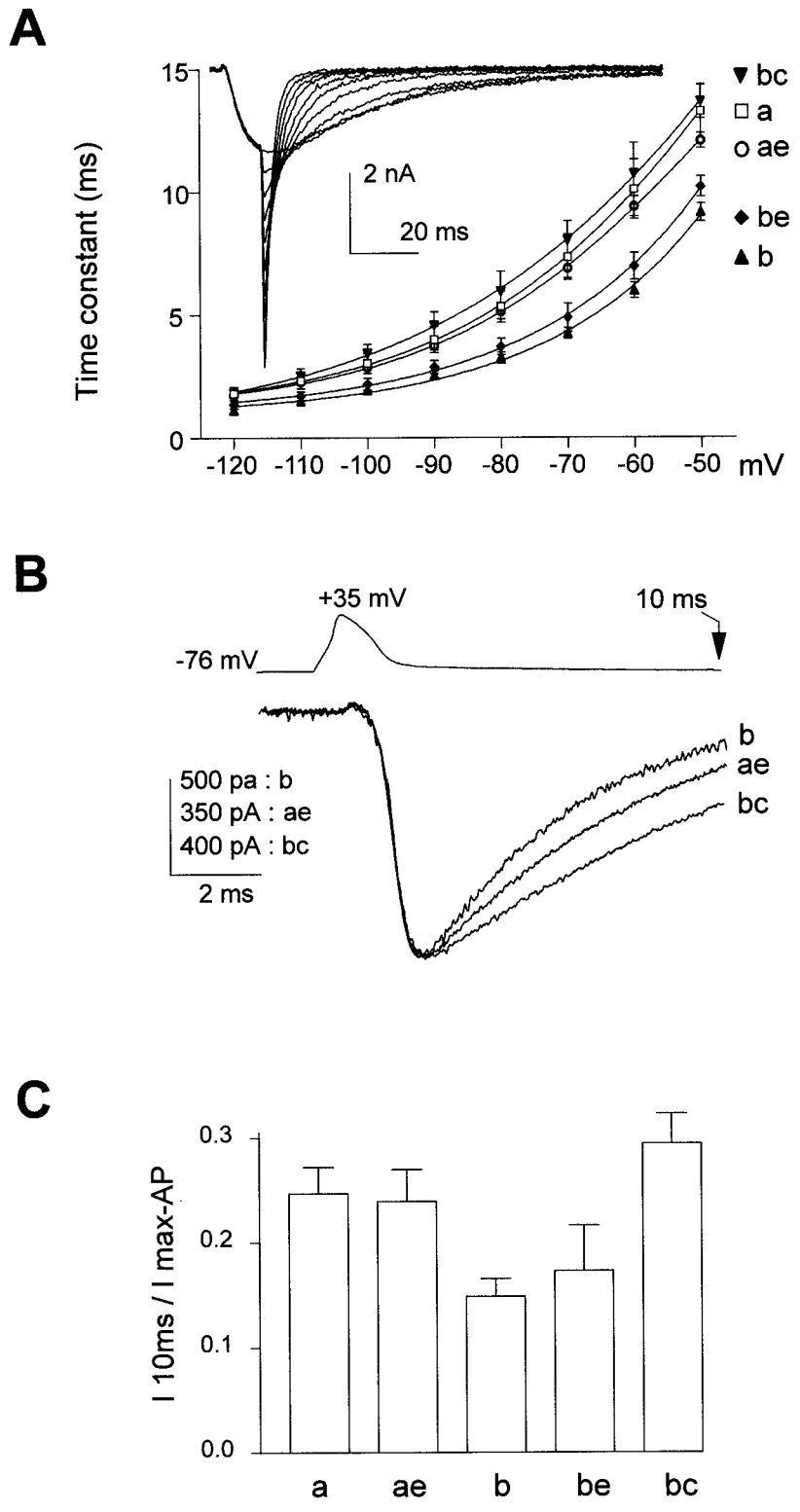

FIGURE 5 Deactivation properties and action potential clamp experiments. (*A*) Channels were fully activated during an 8-ms TP to −30 mV (HP −110mV), as illustrated with $\alpha_{1G\text{-}a}$ currents in the inset. Tail currents, which reflect the deactivation process, were recorded during the repolarization period for various membrane potentials (−120 mV to −50 mV). The plot is of the deactivation time constant as a function of the repolarization potential. (*B*) To further evaluate the influence of the deactivation properties on the channel activity, action potential (AP) clamp experiments were performed. The figure shows an example of traces obtained for three isoforms that exhibit distinct deactivation properties (*bc*, *ae*, and *b*). (*C*) The decay of the Ca^{2+} entry was then estimated for each isoform by calculating the ratio of the amplitude of the current 10 ms after the beginning of the stimulus (I_{10ms}, see *arrow*) over the maximum amplitude of the AP ($I_{max\text{-}AP}$). According to the deactivation properties, Ca^{2+} entry is more transient for the *b* and *be* isoforms than for the *a* and *ae* isoforms. The *bc* isoform exhibits the slowest decay of the Ca^{2+} entry.

especially in thalamus (~50%). Our data point out that the presence of the insertion e significantly affects channel inactivation. Steady-state inactivation ($V_{0.5}$) was ~5 mV more negative and inactivation kinetics were faster for $\alpha_{1G\text{-}ae}$ and $\alpha_{1G\text{-}be}$ channels compared with $\alpha_{1G\text{-}a}$ and $\alpha_{1G\text{-}b}$ channels. In addition, recovery from inactivation was slightly slower for +e isoforms at negative potential (HP −110 mV) but normalized at more positive membrane

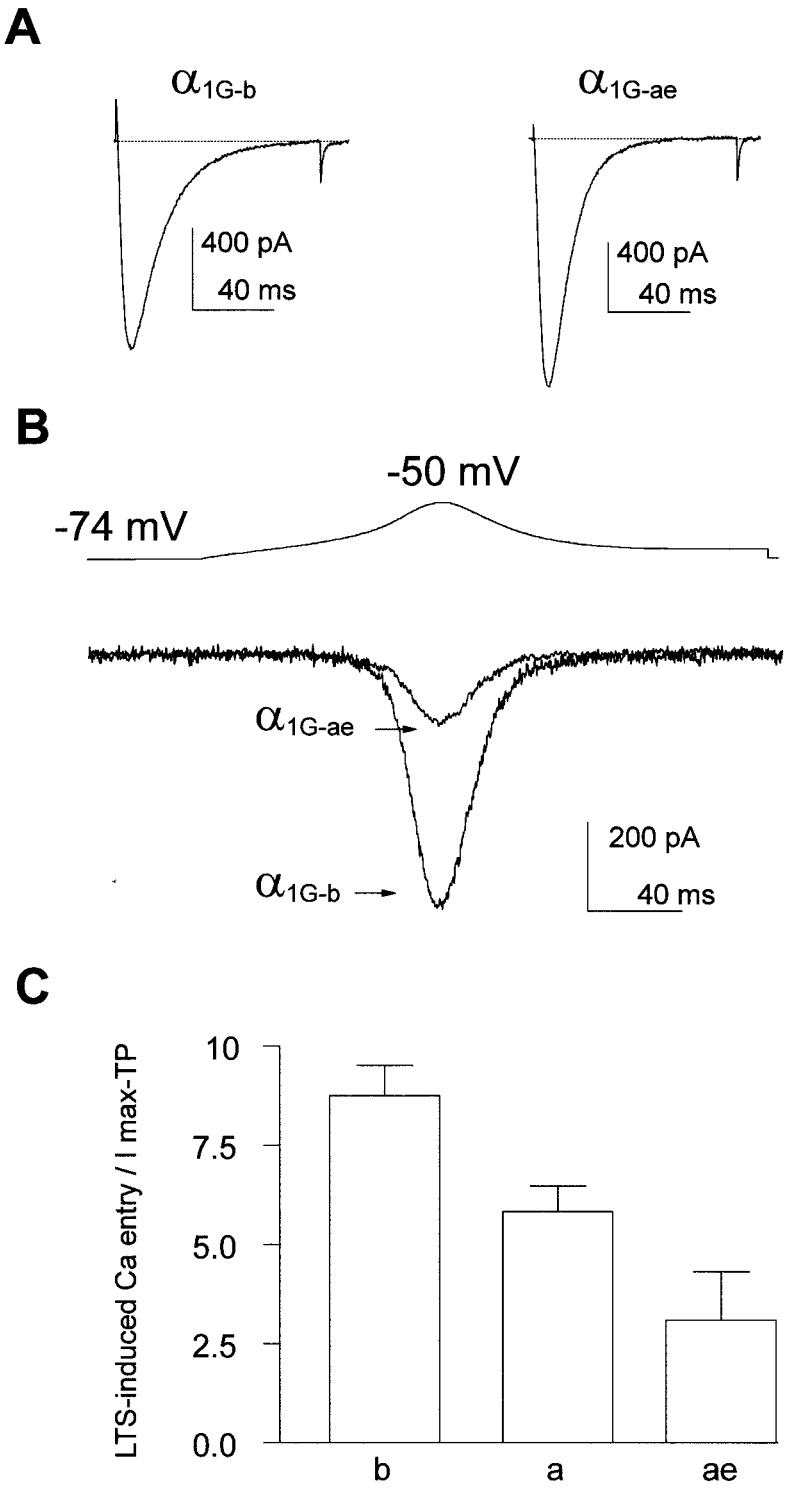

FIGURE 6 Ca^{2+} currents related to α_{1G-a}, α_{1G-ae} and α_{1G-b} isoforms during a mimicked low-threshold spike (LTS). (*A*) Reference current traces obtained for these channel isoforms when recorded for TP at −30 mV from a HP of −110 mV (I_{max-TP}). (*B*) These cells were then recorded during a voltage-clamped LTS generated using the NEURON model. Note that the LTS-induced Ca^{2+} current is more important for α_{1G-b} versus α_{1G-ae} channels, whereas no differences were observed for several other parameters (current threshold, time to peak, and kinetics). (*C*) Quantification of the channel availability was performed for α_{1G-b}, α_{1G-a}, and α_{1G-ae} isoforms based on the amount of the Ca^{2+} entry (LTS-induced Ca^{2+} entry in pA ms) normalized to the peak amplitude during the test pulse (I_{max-TP}) shown in *A*.

potential (HP −70 mV). No change in the steady-state activation properties has been observed between +e and −e isoforms. Again, activation and deactivation kinetics were unchanged between these two sets of channels. It is attractive to propose that insertion e in the proximal II-III loop of the α_{1G} subunit could contribute to fast inactivation by acting as a cytoplasmic gating particle. Indeed, this role has been attributed to the III-IV loop of Na^+ channels (Patton et al., 1992) and also proposed for the I-II linker of α_{1A} and α_{1E} Ca^{2+} channels (Herlitze et al., 1997; Stotz et al., 2000). For HVA Ca^{2+} channels several other cytoplasmic determinants could possibly participate to the inactivation pro-

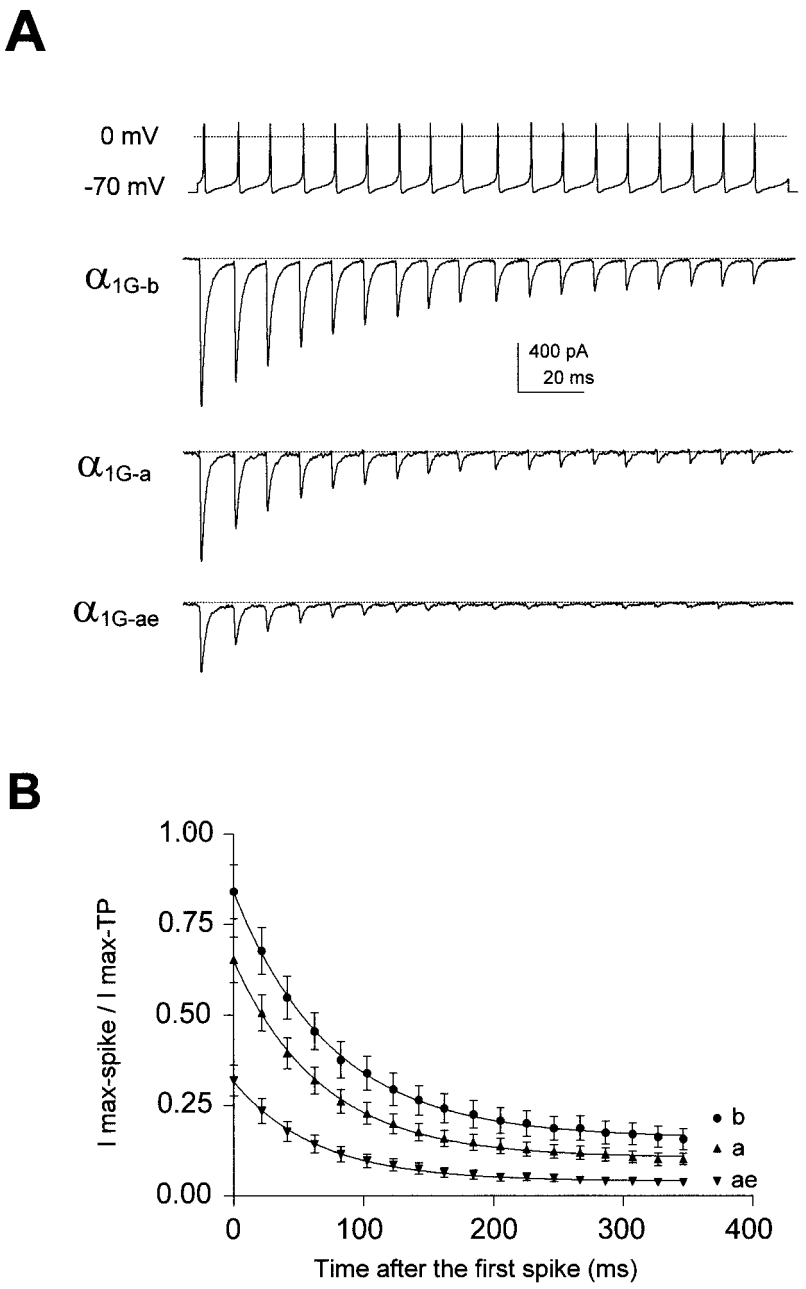

FIGURE 7 Current properties related to $\alpha_{1G\text{-}a}$, $\alpha_{1G\text{-}ae}$, and $\alpha_{1G\text{-}b}$ isoforms during a voltage-clamped train of action potentials, i.e., spikes (50 Hz, HP −76mV) typical of those recorded on spontaneously firing Purkinje fiber. (*A*) The cells described in Fig. 6 were recorded during the train of spikes. The traces show that the largest Ca^{2+} entry occurred via $\alpha_{1G\text{-}b}$ channels, whereas Ca^{2+} entry via *a* isoforms was modest, especially for $\alpha_{1G\text{-}ae}$ channels, inactivated rapidly, and was negligible after the 10th spike. (*B*) The Ca^{2+} entry during the train-of-spike duration is expressed as the ratio of the maximal amplitude of each spike ($I_{max\text{-}spike}$) over the maximal amplitude of a test pulse at −30 mV from a HP of −110 mV ($I_{max\text{-}TP}$) applied to the same cell.

cess. For example, it has been reported that two human α_{1E} isoforms with a distinct II-III loop can generate different inactivation kinetics (Harpold et al., 1998). Also, it has been proposed that the transmembrane IIS6 region of the neuronal α_{1E} channel might serve as a docking site for a cytoplasmic inactivation gate (Stotz et al., 2000). Besides, it was also shown that the II-III loop is critical for interaction with the ryanodine receptor in the case of L-type channels (α_{1S} subunit) (Tanabe et al., 1990) or with syntaxin and SNAP-25 in the case P/Q type channels (α_{1A} subunit) (Rettig et al., 1996). Interestingly, the syntaxin interaction occurs with specific isoforms of α_{1A} channels, suggesting that synaptic transmission could be differentially regulated through the expression of α_{1A} isoforms. Overall, the extensive structure-function studies performed on HVA channels, together with the careful examination of the specific properties of the HVA α_1 isoforms, will certainly provide a basis toward the understanding of the specific properties of the isoforms of the T-type α_{1G} subunit.

The loop between domains III and IV, which originally appeared to be the most conserved intracellular region among the three T-type α_1 subunits (Lee et al., 1999; Monteil et al., 2000a), exhibits several sequence variations as a consequence of alternative splicing of exon 25 that

generate sequence variations a and b. Also, the alternative use of exon 26 encodes an additional 18-amino-acid stretch (variation c). To date, the isoforms $\alpha_{1G\text{-a}}$, $\alpha_{1G\text{-b}}$, and $\alpha_{1G\text{-bc}}$ have been found to be expressed in humans (Monteil et al., 2000a; Mittman et al., 1999b), whereas the isoform $\alpha_{1G\text{-ac}}$ was found only in rodents (Klugbauer et al., 1999). We did not consider the study of an $\alpha_{1G\text{-ac}}$ construct in this analysis because in our hands, as well as for others (Mittman et al., 1999b), no evidence for $\alpha_{1G\text{-ac}}$ expression was found in humans. Considering the human brain mRNA samples analyzed in Monteil et al. (2000a), a majority of isoforms containing the a variation was found (~75%), with $\alpha_{1G\text{-a}}$ being preferentially retrieved in cerebellum (~80%) and in whole brain (~35%). Comparison of the functional properties of the $\alpha_{1G\text{-a}}$ and $\alpha_{1G\text{-b}}$ isoforms has revealed significant differences in activation and inactivation properties. A major consequence of the alternative splicing of exon 25, which removes seven amino acids to provide $\alpha_{1G\text{-b}}$, is a 5-mV shift in the steady-state activation properties with $\alpha_{1G\text{-a}}$ channels being activated at more negative potential. Similarly, a significant leftward shift (~10 mV) in the steady-state inactivation was retrieved between these two channel isotypes. In addition, activation and inactivation kinetics were significantly slower for the current generated by $\alpha_{1G\text{-b}}$ channels, whereas deactivation kinetics of $\alpha_{1G\text{-b}}$ current was faster. Finally, recovery from inactivation was also significantly faster for the current generated by $\alpha_{1G\text{-b}}$ compared with $\alpha_{1G\text{-a}}$ current. Altogether these data strongly indicate that the gating properties markedly differ among the $\alpha_{1G\text{-a}}$ and $\alpha_{1G\text{-b}}$ channels. Similar electrophysiological patterns were retrieved between $\alpha_{1G\text{-be}}$ and $\alpha_{1G\text{-ae}}$ isoforms. The role of insertion c was deduced from the comparison of the properties of $\alpha_{1G\text{-b}}$ and $\alpha_{1G\text{-bc}}$ channels. The currents generated by $\alpha_{1G\text{-bc}}$ channels exhibit a significant 5-mV leftward shift in their steady-state inactivation but no difference in their steady-state activation properties. In addition, $\alpha_{1G\text{-bc}}$ currents display similar activation and inactivation kinetics but significantly slower deactivation. Recovery from inactivation was also slower for $\alpha_{1G\text{-bc}}$ current compared with $\alpha_{1G\text{-b}}$ current. It is therefore important to note that the detailed description of the electrophysiological properties of the $\alpha_{1G\text{-a}}$ and $\alpha_{1G\text{-b}}$ channels and those of $\alpha_{1G\text{-b}}$ and $\alpha_{1G\text{-bc}}$ channels has clearly indicated that the molecular nature of the III-IV loop is essential in the establishment of gating properties of the T-type current generated by the α_{1G} subunit. Again, these results can be discussed in light of the Na^+ or HVA Ca^{2+} channel properties. There is little evidence for the III-IV loop of HVA Ca^{2+} channels being involved in Ca^{2+} channel inactivation (Adams and Tanabe, 1997). By contrast, for Na^+ channels it was clearly demonstrated that the III-IV linker includes an IFM motif critical for fast inactivation (Patton et al., 1992). Although no isoleucine-phenylalanine-methionine motif was retrieved in any of the α_{1G} isoforms, the description of the Na^+ channel inactivation would be more relevant to depict how the intracellular III-IV loop of T-type α_{1G} channels is involved in inactivation. Our data also describe a role for the III-IV region in steady-state activation. To our knowledge, and disregarding the modulation by regulatory subunits (for review, see Walker and De Waard, 1998), a precise involvement in voltage-dependent activation of an intracellular domain of HVA Ca^{2+} channels, especially the III-IV loop, has not been reported. To date our data are best described by a direct involvement of a III-IV intracellular region in voltage-dependent activation as recently suggested for cardiac Na^+ channels (Bennett, 1999). Nevertheless, we cannot exclude that these phenomena occur through the control of any regulatory proteins.

The electrophysiological differences between the α_{1G} variants should be now considered together with the relevant evidence that $\alpha_{1G\text{-a}}$ and $\alpha_{1G\text{-ae}}$ isoforms are the major forms expressed in human brain, especially in the cerebellum and thalamus (Monteil et al., 2000a; Dubin et al., 2000). It is now well documented that T-type channels are important for generating specific types of neuronal activities (Llinas and Yarom, 1981; McCormick and Huguenard, 1992; Aizenman and Linden, 1999; for review see also Gutnick and Yarom, 1989). It was therefore important to investigate the behavior of these channel isoforms using specific voltage-clamped thalamus and cerebellum neuronal activities. Using mimicked thalamic LTS activity, we found that availability of T-type channels is primarily related to their steady-state inactivation properties at the considered membrane potential (HP −74 mV). Similarly, experiments performed with a cerebellar spike train protocol have also indicated that the channel availability for the first spike is correlated to steady-state inactivation, i.e., at HP −70 mV. During the course of the spike train, repetitive depolarizations produce cumulative inactivation that strongly reduced the current amplitude (to ~20% for $\alpha_{1G\text{-b}}$ and less than 5% for $\alpha_{1G\text{-ae}}$ of the initial current amplitude). Although it is unlikely that T-type current would control the firing activity of Purkinje neurons, it has been suggested that Purkinje T-type channels could play some role in spontaneous firing. This role would be even larger if cells would be even more hyperpolarized between spikes (Raman and Bean, 1999). The steady-state inward Ca^{2+} current measured in these experiments could reflect a potential contribution of the T-type currents in firing activity, as suggested by Raman and Bean, 1999. These authors have reported that nearly complete inactivation of the native Purkinje T-type currents occurs after six spikes. This behavior is in good agreement with our observations with the *a* isoforms. Altogether, both the RT-PCR experiments described in Monteil et al. (2000a) and the electrophysiological data reported here strongly indicate that native Purkinje T-type currents are not *b* isoforms and most likely are predicted to be an $\alpha_{1G\text{-a}}$ isoform.

Overall, our data have pointed out that one consequence of functionally distinct α_{1G} variants might be to adjust the electrogenic coupling of T-type Ca^{2+} signaling with the

neuronal firing or bursting activities. In light of our data, one can predict that the a isoforms, especially $\alpha_{1G\text{-}ae}$ channels that are expressed in thalamus, would show larger de-inactivation following hyperpolarization and could contribute efficiently to shape the rebound bursts typical of thalamic neurons. Such a hypothesis can now be explored on the basis of the present study by stimulating HEK-293 cells overexpressing pure populations of α_{1G} variants with original recordings of specific neuronal activities. Also, it will be possible to simulate isoform-specific T-channel activities in modeling experiments (Destexhe et al., 1998) that would certainly emphasize how much differences in gating kinetics and voltage dependence of activation and inactivation might affect action-potential-induced Ca^{2+} entry. It could help also to specify the contribution of isotype-specific T-type Ca^{2+} currents in light of the other intrinsic membrane currents of the native neurons. Combining these strategies would help to specify the isoform-specific role of α_{1G} channels in bursting or pace-making activities when hyperpolarized membrane potentials are reached as a result of mimicked hyperpolarizing postsynaptic potentials (Aizenman and Linden, 1999).

Interestingly, very little is known regarding the regulatory mechanisms of T-type channels, as compared with HVA Ca^{2+} channels (Huguenard, 1996), but one should note that all the splice variants described to date for the α_{1G} channel differ in intracellular regions: II-III and III-IV loops and C-terminus. T-type channels could be regulated by opioid receptors (Schroeder et al., 1991) or 5-HT receptors (Sun and Dale, 1999). The protein kinase C (PKC) is also suspected to regulate T-type channels (Furukawa et al., 1992; Maturana et al., 1999). It is therefore important to note that splicing of the α_{1G} subunit within the III-IV linker affects a PKA/PKC consensus site that is present in the *a* isoforms but removed in the *b* isoforms (Monteil et al., 2000a). Further investigations should therefore combine molecular strategies (point mutants and deletion mutants) and regulatory studies to test whether the differences in functional properties between isoforms are linked to the intrinsic amino acid composition or regulatory pathways. In addition, the first evidence for subunit regulation of T-type channels has been reported (Dolphin et al., 1999; Hobom et al., 2000), and it will now be important to determine whether such a regulation is isoform specific. Overall, alternative splicing is an important mechanism for generating functionally distinct products from a single gene in different tissues, especially in the nervous system (for review, see Grabowski 1998) and at different stages during development. For T-type α_{1G} channels, the existence of several isoforms might account for cell-specific signaling. In neurons, α_{1G} channels are likely to participate in electrogenic activity whereas in other systems, T-type channels made of α_{1G} subunit could support cellular functions related to an increase in basal Ca^{2+} concentration (Chemin et al., 2000) such as secretion as demonstrated for atrial myocytes (Leuranguer et al., 2000) or gene expression.

In summary, our study has revealed that subtle differences in the gating behavior between T-type α_{1G} splice variants can tune significantly the channel activity. This result strongly indicates that further studies performed on neuronal cells should integrate the molecular nature of the T-type channels in terms of isotypes (α_{1G}, α_{1H}, and α_{1I} subunits) as well as splice variants especially for the α_{1G} subunits. Overall, this is the first demonstration that expression of distinct variants for the T-type α_{1G} subunit can increase diversity of low-voltage-activated currents in the various tissues expressing this subunit.

We are most grateful to S. Spiesser for excellent technical assistance and to S. J. Dubel for critical reading of the final version of the manuscript. We gratefully acknowledge P. Fontanaud for introducing us to the use of the NEURON model and for stimulating discussions and Pierre Charnet.
This work was supported in part by the Programme Génome du CNRS, Association pour la Recherche contre le Cancer (ARC9011), and Association Française contre les myopathies (AFM). A.M. was supported by Produit Roche (France) and the GRRC (Groupe de Réflexion sur la Recherche Cardio-vasculaire).

REFERENCES

Adams, B., and T. Tanabe. 1997. Structural regions of the cardiac Ca channel alpha subunit involved in Ca-dependent inactivation. *J. Gen. Physiol.* 110:379–389.

Aizenman, C. D., and D. J. Linden. 1999. Regulation of the rebound depolarization and spontaneous firing patterns of deep nuclear neurons in slices of rat cerebellum. *J. Neurophysiol.* 82:1697–1709.

Bean, B. P. 1989. Classes of calcium channels in vertebrate cells. *Annu. Rev. Physiol.* 51:367–384.

Bennett, E. S. 1999. Effects of channel cytoplasmic regions on the activation mechanisms of cardiac versus skeletal muscle Na(+) channels. *Biophys. J.* 77:2999–3009.

Bourinet, E., T. W. Soong, K. Sutton, S. Slaymaker, E. Mathews, A. Monteil, G. W. Zamponi, J. Nargeot, and T. P. Snutch. 1999. Splicing of alpha 1A subunit gene generates phenotypic variants of P- and Q-type calcium channels. *Nat. Neurosci.* 2:407–415.

Carbone, E., and H. D. Lux. 1984. A low-voltage-activated, fully inactivating Ca channel in vertebrate sensory neurons. *Nature.* 310:501–502.

Chemin, J., A. Monteil, C. Briquaire, S. Richard, E. Perez-Reyes, J. Nargeot, and P. Lory. 2000. Overexpression of T-type calcium channels in HEK-293 cells increases intracellular calcium without affecting cellular proliferation. *FEBS Lett*. 478:166–172.

Chen, C. F., and P. Hess. 1990. Mechanism of gating of T-type calcium channels. *J. Gen. Physiol.* 96:603–630.

Cribbs, L. L., J. C. Gomora, A. N. Daud, J. Lee, and E. Perez-Reyes. 2000. Molecular cloning and functional expression of Ca(v)3.1c, a T-type calcium channel from human brain. *FEBS Lett.* 466:54–58. Corrigendum. *FEBS Lett.* 470:378.

Cribbs, L. L., J. H. Lee, J. Yang, J. Satin, Y. Zhang, A. Daud, J. Barclay, M. P. Williamson, M. Fox, M. Rees, and E. Perez-Reyes. 1998. Cloning and characterization of alpha1H from human heart, a member of the T-type Ca^{2+} channel gene family. *Circ. Res.* 83:103–109.

Destexhe, A., M. Neubig, D. Ulrich, and J. Huguenard. 1998. Dendritic low-threshold calcium currents in thalamic relay cells. *J. Neurosci.* 18:3574–3588.

Dolphin, A. C., C. N. Wyatt, J. Richards, R. E. Beattie, P. Craig, J. H. Lee, L. L. Cribbs, S. G. Volsen, and E. Perez-Reyes. 1999. The effect of

alpha2-delta and other accessory subunits on expression and properties of the calcium channel alpha1G. *J. Physiol. (Lond.).* 519:35–45.

Dubin, A. E., J. Pyati, J. Y. Zhu, J. E. Galindo, R. Huvar, M. R. Jackson, M. G. Erlander, and R. W. Johnson. 2000. Novel isoform of a T-type alpha1G calcium channel isolated from human thalamus. *Biophys. J.* 78:459A.

Furukawa, T., H. Ito, J. Nitta, M. Tsujino, S. Adachi, M. Hiroe, F. Marumo, T. Sawanobori, and M. Hiraoka. 1992. Endothelin-1 enhances calcium entry through T-type calcium channels in cultured neonatal rat ventricular myocytes. *Circ. Res.* 71:1242–1253.

Grabowski, P. J. 1998. Splicing regulation in neurons: tinkering with cell-specific control. *Cell.* 92:709–712.

Gutnick, M. J., and Y. Yarom. 1989. Low threshold calcium spikes, intrinsic neuronal oscillation and rhythm generation in the CNS. *J. Neurosci. Methods.* 28:93–99.

Harpold, M. M., M. E. Williams, P. F. Brust, K. Stauderman, A. Urrutia, E. C. Johnson, and M. Hans. 1998. Human neuronal voltage-gated calcium channels: splice variants, subunit interactions and subtypes. *In* Low-Voltage-Activated T-type Calcium Channel. R. W. Tsien, J. P. Clozel, and J. Nargeot, editors. ADIS International, Chester, UK. 218–228

Herlitze, S., G. H. Hockerman, T. Scheuer, and W. A. Catterall. 1997. Molecular determinants of inactivation and G protein modulation in the intracellular loop connecting domains I and II of the calcium channel alpha1A subunit. *Proc. Natl. Acad. Sci. U.S.A.* 94:1512–1516.

Hines, M. L., and N. T. Carnevale. 1997. The NEURON simulation environment. *Neural Comput.* 9:1179–1209.

Hobom, M., S. Dai, E. Marais, L. Lacinova, F. Hofmann, and N. Klugbauer. 2000. Neuronal distribution and functional characterization of the calcium channel alpha2delta-2 subunit. *Eur. J. Neurosci.* 12:1217–1226.

Huguenard, J. R. 1996. Low-threshold calcium currents in central nervous system neurons. *Annu. Rev. Physiol.* 58:329–348.

Klockner, U., J. H. Lee, L. L. Cribbs, A. Daud, J. Hescheler, A. Pereverzev, E. Perez-Reyes, and T. Schneider. 1999. Comparison of the Ca^{2+} currents induced by expression of three cloned alpha1 subunits, alpha1G, alpha1H and alpha1I, of low-voltage-activated T-type Ca^{2+} channels. *Eur. J. Neurosci.* 11:4171–4178.

Klugbauer, N., E. Marais, L. Lacinova, and F. Hofmann. 1999. A T-type calcium channel from mouse brain. *Pflugers Arch.* 437:710–715.

Kozlov, A. S., F. McKenna, J. H. Lee, L. L. Cribbs, E. Perez-Reyes, A. Feltz, and R. C. Lambert. 1999. Distinct kinetics of cloned T-type Ca^{2+} channels lead to differential Ca^{2+} entry and frequency-dependence during mock action potentials. *Eur. J. Neurosci.* 11:4149–4158.

Lambert, R. C., F. McKenna, Y. Maulet, E. M. Talley, D. A. Bayliss, L. L. Cribbs, J. H. Lee, E. Perez-Reyes, and A. Feltz. 1998. Low-voltage-activated Ca^{2+} currents are generated by members of the CavT subunit family (alpha1G/H) in rat primary sensory neurons. *J. Neurosci.* 18: 8605–8613.

Lee, J. H., A. N. Daud, L. L. Cribbs, A. E. Lacerda, A. Pereverzev, U. Klockner, T. Schneider, and E. Perez-Reyes. 1999. Cloning and expression of a novel member of the low voltage-activated T-type calcium channel family. *J. Neurosci.* 19:1912–1921.

Leuranguer, V., A. Monteil, E. Bourinet, G. Dayanithi, and J. Nargeot. 2000. T-type calcium currents in rat cardiomyocytes during post natal development: contribution in hormone secretion. *Am. J. Physiol. Heart Circ. Physiol.* 279:H2540–H2548.

Lin, Z., Y. Lin, S. Schorge, J. Q. Pan, M. Beierlein, and D. Lipscombe. 1999. Alternative splicing of a short cassette exon in alpha1B generates functionally distinct N-type calcium channels in central and peripheral neurons. *J. Neurosci.* 19:5322–5331.

Llinas, R., and Y. Yarom. 1981. Properties and distribution of ionic conductances generating electroresponsiveness of mammalian inferior olivary neurones in vitro. *J. Physiol. (Lond.).* 315:569–584.

Maturana, A. D., M. M. Burnay, A. M. Capponi, M. B. Vallotton, and M. F. Rossier. 1999. Angiotensin II type 1 receptor activation modulates L- and T-type calcium channel activity through distinct mechanisms in bovine adrenal glomerulosa cells. *J. Recept. Signal. Transduct. Res.* 19:509–520.

McCormick, D. A., and J. R. Huguenard. 1992. A model of the electrophysiological properties of thalamocortical relay neurons. *J. Neurophysiol.* 68:1384–1400.

Monteil, A., J. Chemin, E. Bourinet, G. Mennessier, P. Lory, and J. Nargeot. 2000a. Molecular and functional properties of the human alpha(1G) subunit that forms T-type calcium channels. *J. Biol. Chem.* 275:6090–6100.

Monteil, A., J. Chemin, V. Leuranguer, C. Altier, G. Mennessier, E. Bourinet, P. Lory, and J. Nargeot. 2000b. Specific properties of T-type calcium channels generated by the human alpha 1I subunit. *J. Biol. Chem.* 275:16530–16535.

Monteil, A., J. Chemin, E. Bourinet, J. Nargeot, and P. Lory. 2000c. Identification of multiple human alpha1G isoforms of T-type calcium channel with distinct functional properties. *Biophys. J.* 78:199A.

Mittman, S., J. Guo, M. C. Emerick, and W. S. Agnew. 1999a. Structure and alternative splicing of the gene encoding alpha1I, a human brain T calcium channel alpha1 subunit. *Neurosci. Lett.* 269:121–124.

Mittman, S., J. Guo, and W. S. Agnew. 1999b. Structure and alternative splicing of the gene encoding alpha1G, a human brain T calcium channel alpha1 subunit. *Neurosci. Lett.* 274:143–146.

Patton, D. E., J. W. West, W. A. Catterall, and A. L. Goldin. 1992. Amino acid residues required for fast Na(+)-channel inactivation: charge neutralizations and deletions in the III-IV linker. *Proc. Natl. Acad. Sci. U.S.A.* 89:10905–10909.

Perez-Reyes, E., L. L. Cribbs, A. Daud, A. E. Lacerda, J. Barclay, M. P. Williamson, M. Fox, M. Rees, and J. H. Lee. 1998. Molecular characterization of a neuronal low-voltage-activated T-type calcium channel. *Nature.* 391:896–900.

Raman, I. M., and B. P. Bean. 1999. Ionic currents underlying spontaneous action potentials in isolated cerebellar Purkinje neurons. *J. Neurosci.* 19:1663–1674.

Randall, A. D., and R. W. Tsien. 1997. Contrasting biophysical and pharmacological properties of T-type and R-type calcium channels. *Neuropharmacology.* 36:879–893.

Rettig, J., Z. H. Sheng, D. K. Kim, C. D. Hodson, T. P. Snutch, and W. A. Catterall. 1996. Isoform-specific interaction of the alpha1A subunits of brain Ca^{2+} channels with the presynaptic proteins syntaxin and SNAP-25. *Proc. Natl. Acad. Sci. U.S.A.* 93:7363–7368.

Schroeder, J. E., P. S. Fischbach D. Zheng, and E. W. McCleskey. 1991. Activation of mu opioid receptors inhibits transient high- and low-threshold Ca^{2+} currents, but spares a sustained current. *Neuron.* 6:13–20.

Serrano, J. R., E. Perez-Reyes, and S. W. Jones. 1999. State-dependent inactivation of the alpha1G T-type calcium channel. *J. Gen. Physiol.* 114:185–201.

Soldatov, N. M., R. D. Zuhlke, A. Bouron, and H. Reuter. 1997. Molecular structures involved in L-type calcium channel inactivation. Role of the carboxyl-terminal region encoded by exons 40–42 in alpha1C subunit in the kinetics and Ca^{2+} dependence of inactivation. *J. Biol. Chem.* 272: 3560–3566.

Stotz, S. C., J. Hamid, R. L. Spaetgens, S. E. Jarvis, and G. W. Zamponi. 2000. Fast inactivation of voltage-dependent calcium channels: a hinged-lid mechanism. *J. Biol. Chem.* 275:24575–24582.

Sun, Q. Q., and N. Dale. 1999. G-proteins are involved in 5-HT receptor-mediated modulation of N- and P/Q- but not T-type Ca^{2+} channels. *J. Neurosci.* 19:890–899.

Tanabe, T., K. G. Beam, B. A. Adams, T. Niidome, and S. Numa. 1990. Regions of the skeletal muscle dihydropyridine receptor critical for excitation-contraction coupling. *Nature.* 346:567–569.

Walker, D., and M. De Waard. 1998. Subunit interaction sites in voltage-dependent calcium channels: role in channel function. *Trends Neurosci.* 21:148–154.

Williams, M. E., M. S. Washburn, M. Hans, A. Urrutia, P. F. Brust, P. Prodanovich, M. M. Harpold, and K. A. Stauderman. 1999. Structure and functional characterization of a novel human low-voltage activated calcium channel. *J. Neurochem.* 72:791–799.

Zhuravleva, S. O., P. G. Kostyuk, and Y. M. Shuba. 1999. Divalent cation selectivity of the subtypes of low voltage-activated Ca^{2+} channels in thalamic neurons. *Neuroreport.* 10:651–657.